Parrow Matthew (Orcid ID: 0000-0002-3197-2510)

QUANTITATIVE NUCLEAR DNA CONTENT AND CELL CYCLE ANALYSIS OF A MIXOTROPHIC DINOFLAGELLATE BY IMAGE CYTOMETRY

Erik L. J. E. Broemsen [1], Allen R. Place [2], Matthew W. Parrow [1*]

[1] Department of Biological Sciences, University of North Carolina at Charlotte, 9201 University City Blvd., Charlotte, NC 28223, USA.

[2] Institute of Marine and Environmental Technology, University of Maryland Center for Environmental Sciences, 701 E. Pratt Street, Baltimore, MD 21202, USA.

[*] Corresponding author:

Department of Biological Sciences

University of North Carolina at Charlotte

9201 University City Blvd., Charlotte, NC 28223

Email: mwparrow@uncc.edu

Telephone: 704-687-7779

Running Head: Image cytometry of a dinoflagellate

Key index words: Cell cycle; DNA quantification; flow cytometry; image cytometry; in situ growth rate

Abstract**:**

The goal of this work was to develop and demonstrate the utility of microscope-based image cytometry (ICM) as a method for quantifying nuclear DNA content and cell cycle phase distribution in microalgae both in culture and in natural blooms, as an alternative to flow cytometry (FCM). To do so, aliquots from the same samples of the dinoflagellate *Karlodinium veneficum* were examined using both ICM and FCM. Image cytometry specimen preparation and data acquisition methods were optimized to improve precision and agreement between the two techniques. Accuracy and precision of DNA measurements by ICM were significantly higher using the DNA fluorophore DAPI compared to SYBR® Green I. Milli-Q H_2O was found to be superior to Tris-EDTA as a staining and slide preparation solution for ICM analyses. Lower-powered objective magnification (10x, 20x) in image acquisition for ICM produced higher precision in nuclear DNA measurements. Overall precision of ICM analysis of DAPI-stained *Karlodinium veneficum* cells was comparable to FCM, with respective 1C DNA peak coefficients of variation as low as 6.2 %. Cell cycle distributions of mid-log culture samples analyzed by both ICM and FCM were in agreement (Two-way ANOVA; $p = 0.93$); while distributions analyzed in a field sample were similar but not identical (Z-test; $p < 0.001$). Overall, the results show the feasibility of image cytometry as a useful tool for microalgal cell cycle analysis, with the potential for more flexible application to mixotrophic/phagotrophic species and complex field populations.

Introduction

The measurement of phytoplankton growth rates in the field is important for understanding how populations respond to environmental factors during blooms. Several methods have been described for determining species-specific in situ growth rates of phytoplankton in natural blooms, all of which calculate rates based on the frequency of dividing cells, or the frequency of cells within two consecutive terminal stages of cell division and the duration of time between those stages (McDuff & Chisholm, 1982, Carpenter & Chang, 1988, Vaulot, 1992, Chang & Dam, 1993). The cell cycle method described by Carpenter and Chang (1988) provides one of the most accurate approaches based on its use of cell cycle phases S and G2 + M as the consecutive terminal stages. This approach provides advantages over other methods, which rely on morphological identification of proliferation stages (e.g. cells undergoing cytokinesis or binucleated cells) and *a priori* knowledge of the duration of these stages (Litaker et al., 2002). The cell cycle method requires neither of these, but instead depends upon quantitative determination of cellular DNA content and assignment of cells in the population to G1, S, or G2 + M phases.

Fluorescent quantification of cellular DNA content by flow cytometry (FCM) is the gold standard for cell cycle analysis. However, mixotrophic microalgae such as *Karlodinium veneficum* that consume other phytoplankton cells may contain significant non-nuclear DNA in phagocytic food vacuoles, along with their organellar DNA in mitochondria and plastids. Flow cytometry cannot distinguish cytoplasmic from nuclear DNA when analyzing whole cells. Furthermore, natural field populations of microalgae typically exist in a complex assemblage of phototrophic, heterotrophic, and mixotrophic protists that can overlap in cell size and DNA

content, making a target species difficult to separate out for cell cycle analysis by FCM, particularly when the target species is not numerically dominant in the community. These factors have limited the use of FCM for cell cycle analysis of field populations of microalgae, with notable exceptions (Boucher et al., 1991, Vaulot & Partensky, 1992, Liu et al., 1998), and provided the impetus for using microfluorometry instead (Vaulot & Partensky, 1992, Yamaguchi, 1992, Liu et al., 1997, Garcés et al., 1998, Garcés et al., 1999, Gisselson et al., 1999, Van Dolah & Leighfield, 1999, Garcés & Masó, 2001). Microfluorometry is a microscope slide-based technique wherein a light microscope equipped with a fluorescence spectrophotometer is used to allow visual selection and quantitative measurement of stained DNA fluorescence of nuclei in single cells, one cell at a time. A closable aperture allows the operator to optically exclude non-target cells and cytoplasmic DNA. However, this method is time consuming as it requires measurement of one cell at a time, which typically results in only 200- 300 cells being measured and relatively high coefficients of variation (CV; coefficient of variation = [peak SD ÷ mean] ×100) on the fluorescence peaks for G1 and G2 phases (Cetta & Anderson, 1990, Garcés et al., 1998, Garcés et al., 1999, Garcés & Masó, 2001).

An alternative approach to measuring DNA fluorescence by microfluorometry is image cytometry (ICM). This slide-based technique uses a linear charge-coupled device (CCD) camera mounted on a light microscope to acquire digital images of fields of view containing multiple cells with fluorescently stained DNA. These images are then processed with image analysis software to measure fluorescence intensity of all user or software-selected nuclei present in the image. Non-target cells and even non-nuclear DNA in target cells can be simply ignored by manual or software-trained selection of the nuclei of interest. This technique offers all the

advantages of microfluorometry over flow cytometry for complex cells and samples, with added advantages such as faster data collection and digital storage of the original data (images).

ICM has been used extensively in biomedical research, where it has been shown to have comparable utility for cell cycle analysis as FCM (Galbraith et al., 1991, Wang et al., 1995, Maciorowski et al., 1997, Lamas et al., 2003, Bocsi et al., 2004). Variants of ICM have also been used for cell cycle analysis of two dinoflagellate species (Bhaud et al., 1991, Gisselson et al., 1999) and genome size estimation in *Thalassiosira* spp. diatoms (Von Dassow et al., 2008) and multicellular red algae (Kapraun & Freshwater, 2012, Salvador Soler et al., 2014). However, estimates of precision in measurements, such as 1C DNA peak CV's have rarely accompanied these non-biomedical studies, and overall little effort has been made to optimize methodology and provide comparison to established methods such as FCM on non-clinical cells such as microalgae.

The bloom forming toxic dinoflagellate *K. veneficum* is found in temperate and subtropical coastal seas around the world, where it is responsible for major fish kill events (Deeds et al., 2002, Kempton et al., 2002, Lim et al., 2014). The toxins produced by *K. veneficum*, karlotoxins, have been characterized and can be quantified in cultures and field samples (Deeds & Place, 2006, Bachvaroff et al., 2008, Van Wagoner et al., 2008). Previous studies have shown toxicity of blooms to vary widely, and culture-based studies have observed an inverse relationship between growth rates and toxicity (Deeds et al., 2004, Adolf et al., 2009). While this relationship has yet to be observed in nature, it could explain the variable toxicity observed between *K. veneficum* blooms, and within blooms over time. In order to investigate the relationship between growth rates and toxicity in field blooms, we propose ICM as a useful tool for measuring in situ growth using the cell cycle technique. Here we present an optimized

methodology for performing ICM based cell cycle analysis of *K. veneficum* with direct comparison to FCM analysis. Furthermore, we apply these methods to field samples collected during a 2016 bloom of *K. veneficum* in the Baltimore Inner Harbor, MD to demonstrate the feasibility of applying cell cycle analysis to natural bloom populations of mixotrophic microalgae.

Materials and procedures

Cultures

Strain 2010 IH was clonally isolated in 2010 and identified as *K. veneficum* from the Baltimore Inner Harbor by co-author Place's laboratory based on morphology and identical ITS sequence match to other North American *K. veneficum* isolates. Cultures were maintained at 20 °C in 15 ppt EH-1 enriched artificial seawater with 1 mM Hepes, modified from Berges et al. (2001). Illumination was provided by daylight deluxe fluorescent bulbs on a 12h: 12h L: D schedule with a 100 μE m^{-2} s^{-1} intensity.

Sample preparation

Samples were prepared for ICM and FCM analyses by fixing 50 mL of mid-log *K. veneficum* culture in 5 % formalin and 0.1 % Tween 80 (final concentrations) overnight at 4 °C. Following fixation cells were pelleted at 3,000 g for 10 min, resuspended in 50 mL of 70 % methanol, and incubated overnight in darkness at 4 °C. Methanol extracted cells were then pelleted at 2,000 g for 10 minutes and resuspended in 1 mL TE (10 mM Tris-HCl and 1 mM EDTA) with 0.1 % Tween 80.

Microscope instrumentation

All microscopy and ICM was performed with a Zeiss Axio Observer A1 inverted microscope (Carl Zeiss Microscopy GmbH, Jena Germany) equipped with 10x (NA 0.45), 20x (NA 0.8), and 40x (NA 0.95) Plan Apochromat objectives. Epifluorescence excitation was provided by an HBO 103 W/2 mercury short-arc lamp and excitation and emission wavelengths were selected using either a Zeiss filter set 10 (excitation: 450-490 nm, emission: 515-565 nm, beam splitter: 510 nm) or a Zeiss filter set 49 (excitation: 365 nm, emission: 445/50 nm, beam splitter: 395 nm). Images were captured with a Zeiss Axiocam 506 monochromatic CCD camera with a 2752 x 2208 pixel resolution and a 14- bit pixel depth controlled by Zeiss Zen 2.6 software with image analysis package. Camera exposure times were set initially by autoexposure to a randomly selected field of view for each slide analyzed and the exposure time reduced incrementally until the intensity of all pixels within the image fell within the pixel depth of the image histogram in the Zen 2.6 acquisition software. This ensured utilization of the full dynamic range of the camera.

Image calibration

Even with careful alignment and an apochromatic epi-light train, the mercury arc lamp did not provide a totally even intensity field of excitation light across the entire field of view (e.g. higher excitation intensity in the center compared to the edges). In order to correct for this effect within fluorescent images, each pixel was normalized using a shading reference image. This image was acquired from epi-illumination of a thin film of 10 % fluorescein dissolved in 100 mM $NaHCO_3$ mounted between a microscope slide and a # 1.5 coverslip sealed with clear

nail polish, following Model & Burkhardt (2001) and Varga et al. (2004). A new shading reference was acquired for each imaging session following a 15 minute warm up period for the mercury lamp. Exposure time for the shading reference was automatically selected with the "auto exposure" feature. The shading correction was acquired with the "shading correction" feature on the Zen 2.6 image acquisition tab and applied automatically at the time of acquisition for each image. Flow-Check™ Fluorospheres (Beckman Coulter, Fullerton, CA) were used to verify image calibrations and compare precision of fluorescence measurements between FCM and ICM. A drop of fluorosphere solution was placed on a silicone grease rimmed 25 mm x 25 mm # 1.5 coverslip and mounted to a microscope slide. The slide was placed on the microscope stage with coverslip facing down and fluorospheres allowed to settle on coverslip surface prior to imaging. All imaging sessions were conducted in a darkened room. The microscope light path was directed 100% to the camera, and fields of view were selected in a grid fashion using low-light brightfield displayed on the computer screen. To capture fluorescence images, transmitted light was blocked and epi-illumination triggered for immediate image acquisition.

Image analysis

Images of fluorescently stained cells and fluorosphere standards were analyzed with Zen 2.6 image analysis package. Images were framed for analysis such that the entirety of the image was used and any nuclei touching the edges of the image were excluded from analyses. Images were automatically segmented and fluorescent objects detected by defining the threshold for foreground pixels using the Otsu algorithm and adjacent touching objects were separated using the watershed method (Otsu, 1979, Malpica et al., 1997). Non-target fluorescent objects were then excluded from subsequent analyses based on area (number of pixels x scaling factor; μm^2)

of the object such that only objects between 15 μm^2 and 160 μm^2 (i.e. equivalent circular diameters between 4 µm and 14 µm) were included. Parameters recorded for each target fluorescent object in each image were area, Feret ratio (the ratio of the minimum and maximum distances between two parallel lines tangent to the object perimeter), and Integrated fluorescence intensity (sum of pixel values).

Methods optimization

In order to optimize ICM methodology several factors in sample preparation and instrumentation were considered and compared. These factors included selection of nucleic acid dye (SYBR® Green I [Lonza Rockland, Rockland, ME] vs 4′, 6 – diamidino – 2 – phenylindole; DAPI), cell resuspension/slide preparation buffer (TE buffer vs Milli-Q H_2O), and microscope objective magnification power (10x vs 20x vs 40x) used in image acquisition. Genome size estimation and 1C DNA peak CV's, as determined by ICM and FCM, served as metrics for comparison and method selection.

For dye comparison, cell suspensions were diluted to 1 x 10^5 cells mL^{-1} in TE buffer with 1 x 10^5 calf thymocyte nuclei as a genome size standard (7.4 pg DNA $nucleus^{-1}$, Biosure, Grass Valley, CA) and stained with either SYBR® Green (5x and 20x concentrations, diluted from 10,000x stock concentration) or DAPI (1 µg mL^{-1}) fluorescent nucleic acid dyes (final concentrations) (Vinogradov, 1998). For each cell suspension 20 µL was aliquoted onto a poly-D-lysine coated coverslip (Electron Microscopy Sciences, Hatfield, PA) and allowed to fully air dry. Coverslips were then mounted onto microscope slides with 10 µL Vectashield® antifade (Vector Laboratories, Burlingame, CA) and sealed with clear nail polish. Slides were then subject to ICM analysis and remaining suspensions were analyzed by FCM with a BD

LSRFortessa™ flow cytometer (BD Biosciences, San Jose, California) equipped with 405 nm and 488 nm 50 mW solid-state lasers following methods of Kremp & Parrow (2006). Suspensions stained with DAPI were analyzed using the 405 nm laser for excitation and fluorescence emissions were detected at 450 nm. SYBR® Green I stained suspensions were analyzed with the 488 nm laser and fluorescence emissions were detected at 530 nm.

Selection of optimal cell resuspension/slide preparation buffer and objective power were combined into one set of comparisons. *Karlodinium veneficum* cells were harvested and prepared as above and diluted to 1 x 10^5 cells mL^{-1} in either TE or Milli-Q H2O and stained with 1 μg mL^{-1} DAPI. Slides were prepared as above and ICM analysis was performed on images captured with 10x, 20x, and 40x objectives. Coefficients of variation on 1C DNA peaks (G1 phase cells) were compared to determine optimal buffer and magnification power for ICM.

Comparing ICM and FCM for cell cycle analysis

Titrations to determine optimal dye concentration were carried out by comparative genome size estimation between ICM and FCM using calf thymocyte nuclei as a genome size standard. Samples were diluted in Milli-Q H_2O to 2.6 x 10^5 *K. veneficum* cells mL^{-1}, calf thymocyte nuclei were added to a concentration of 1 x 10^5 calf thymocyte nuclei mL^{-1}, and stained with 1 μg mL^{-1}, 2 μg mL^{-1}, and 4 μg mL^{-1} DAPI (final concentrations). For ICM, 20 μL of each cell suspension was aliquoted onto a poly-D-lysine-coated coverslip and allowed to air dry. Dried coverslips were mounted onto microscope slides with 10 μL of Vectashield® antifade mounting medium (Vector Laboratories, Burlingame, CA) and sealed with clear nail polish. Remaining cell suspensions were directly used for FCM analysis with a BD LSRFortessa™ flow cytometer. Genome sizes and associated error were calculated from single cytometry

experiments without replication. *Karlodinium veneficum* was assumed to be haplontic in life cycle (Adolf et al., 2020), and so the signal mean of the lowest measured DNA fluorescence peak of flagellate cells was assumed to represent 1C DNA (1N, G1 cell cycle phase) following Kremp & Parrow (2006). Genome sizes were determined by multiplying the mean fluorescence ratio of 1C DNA *K. veneficum* cells: calf thymocyte nuclei by the 2C value of *Bos taurus*.

For cell cycle analysis a single culture was harvested at mid-log and prepared as described above. In triplicate this cell suspension was diluted in Milli-Q H_2O to 2.6 x 10^5 *K. veneficum* cells mL^{-1} and genome size standards were added at 1 x 10^5 calf thymocyte nuclei mL^{-1}; the suspension was then stained with DAPI (1 μg mL^{-1}). Microscope slides were prepared as described above and the remaining cell suspensions were subjected to FCM analysis as above. ICM and FCM DNA histograms from replicate samples were deconvoluted to estimate cell cycle phase distributions using FlowJo V10.6 (FlowJo, Ashland, Oregon).

Field samples were collected during a *K. veneficum* dominated mixed species algal bloom occurring in the Baltimore Inner Harbor, MD on June 3rd, 2016. Bloom samples were fixed with 5 % formalin and 0.1 % Tween 80 and processed identically to culture samples. Following dilution into Milli-Q H_2O and prior to staining with DAPI (1 μg mL^{-1}), cells were passed through a 35 μm Nitex® mesh in order to remove larger plankton and debris. Following DAPI staining, the cell suspension was mounted on poly-D-lysine coated coverslips as described above. Images used for ICM analysis were collected with the 20x objective. The remaining cell suspension was subjected to FCM analysis and the presumptive *K. veneficum* population was gated using forward scatter vs side scatter gates established from culture samples of *K. veneficum*, as in Van Dolah et al. (2008).

Data collection methods and statistics

All images were saved as Zeiss proprietary file format (.CZI). Following image analysis, all data were exported as comma delimited .CSV file format and data from multiple fields of view were concatenated together using Windows 10 command prompt. Concatenated data were imported directly into FlowJo, which automatically converted the .CSV files into Flow Cytometry Standard (.FCS) file format. In order to maintain comparability between FCM and ICM measurements, the number of events analyzed by either method were restricted to comparable quantities. This was achieved by randomly subsampling analyses to equal number of events by using the FlowJo utilities plugin tool DownSample, or by stopping FCM analyses at the first 2500 events. Peak means, CV's, and proportions of cell cycle phases were determined using FlowJo following the Watson-Pragmatic model for phase deconvolution (Watson et al., 1987). ICM versus FCM data were compared by Two-way ANOVA in GraphPad Prism 6 (GraphPad Software, San Diego, California). Calculation of confidence intervals and Z-test statistics were performed in Microsoft® Excel® software 2013 (Microsoft Corporation, Redmond, Washington).

Assessment

Precision of quantitative fluorescence measurements

Precise measurement of DNA content by ICM was significantly impacted by uneven sample illumination provided by the epifluorescence light source. The effect of this uneven illumination is shown in Figures 1A - D, where the homogenous film of 10 % fluorescein was epi-illuminated by the microscope mercury arc lamp. Regions of brighter (center) pixels and

more dim (edges) pixels illustrate the positional effect such a pattern had on the fluorescence intensity of uncorrected images (Fig. 1A). This was also evident in the 2.5 dimensional projection of the image (Fig. 1C), where the pixel intensity (i.e. fluorescence) was visualized on the Z-axis. Flatfield correction of this uneven illumination pattern (Fig. 1B and 1D) was carried out by normalizing data images using the methods described above. Statistical analysis also supported the necessity of flatfield correction: mean pixel intensity of a representative uncorrected image of 10 % fluorescein had a fluorescence intensity of 11299.0 ± 1771.1 gray-levels resulting in a fluorescence peak CV of 15.7 %. Upon flatfield correction mean pixel intensity of the same image increased to 15071.9 ± 184.0 gray-levels with a corresponding peak CV of 1.2 %. Fluorescence intensity of Flow-Check™ fluorospheres (n = 1373) was analyzed by both FCM (Fig. 2A) and ICM with (Fig. 2B) and without (Fig. 2C) flatfield correction. Peak CV's for ICM with and without correction resulted in CVs of 2.1 % and 11.7 %, respectively. Peak CV's for FCM analyzed fluorospheres was 1.8 %.

Methods optimization

Not all SYBR® Green I and DAPI staining treatments produced equivalent DNA histograms within and between ICM and FCM analyses (Fig. 3). The lowest ICM CV for the internal calf thymocyte nuclei DNA standard was 8.1 % when stained with the 20x concentration of SYBR® Green I (Table 1). The lowest FCM CV for the calf thymocyte nuclei was 2.5 % when stained with DAPI. The CVs for calf thymocyte nuclei were lower for FCM analyses than ICM with the exception of the 20x Concentration of SYBR® Green I. The lowest ICM and FCM *K. veneficum* 1C DNA peak CVs were 5.8 % and 3.3 %, respectively, when stained with DAPI. The highest was 16.6 % with 20x SYBR® Green I staining. As with the calf thymocyte nuclei

CVs, *K. veneficum* 1C DNA peak CVs were lowest when analyzed by FCM, with the exception of the 20x SYBR® Green I concentration. Furthermore, genome size estimations only agreed between the SYBR® Green I FCM and DAPI ICM analyses, while the DAPI FCM genome size estimation was not in agreement with any SYBR® Green I analyses or the DAPI ICM analysis.

Both objective magnification and slide preparation solution had significant effects on DNA measurement precision in ICM (Fig. 4). Coefficients of variation for both Milli-Q H2O and TE buffer increased with objective magnification power (respective coefficients of correlation, r = 0.99 and 0.97). The CVs for data collected with the 10x objective were similar for Milli-Q H_2O and TE buffer (5.4 % and 5.5 %, respectively), however, as objective magnification increased the disparity between Milli-Q H_2O and TE buffer CVs increased (Fig. 4). Additionally, CVs for cells resuspended in TE buffer were greater than those in Milli-Q H2O. The effect of magnification and slide preparation solution was also apparent in the number of images needed to capture comparable numbers of cells between the comparisons. The number of images required to reach the target sample size increased with magnification due to smaller fields of view, and was also higher for slides prepared with TE buffer compared to Milli-Q H2O at each magnification (Fig. 4). This was caused by salt precipitation from the TE buffer during slide preparation, which caused the cells to settle on the coverslip in slightly different focal planes.

Fluorescent dye titrations

Titrations revealed that as concentrations of DAPI increased, estimated genome sizes decreased for FCM, with the highest estimate at 12.6 ± 0.8 pg DNA $cell^{-1}$ and the lowest at 7.7 ± 1.4 pg DNA $cell^{-1}$ (Fig. 5). Additionally, FCM CVs for *K. veneficum* 1C DNA peaks increased

with DAPI concentrations from 5.3 % to 16.7 %. Calf thymocyte nuclei CVs remained low only increasing at the highest DAPI concentration (5.6 % at 4 µg mL^{-1}).

Unlike FCM, ICM-based genome size measurements for *K. veneficum* varied by less than 1.0 pg DNA $cell^{-1}$ across the different DAPI concentration treatments (Fig. 5). Image cytometry CVs for *K. veneficum* 1C DNA peaks remained below 10 % at all concentrations, but did increase with increasing DAPI concentrations (6.2 %, 7.5 %, and 9.3 % at 1 µg mL^{-1}, 2 µg mL^{-1}, and 4 µg mL^{-1}, respectively). Calf thymocyte nuclei CVs were only below 10 % at the lowest concentration of DAPI tested (8.3 % at 1 µg mL^{-1}). Optimal DAPI concentration for cell cycle analysis (1 µg mL^{-1}) was chosen from the above titrations where genome size estimation was in closest agreement between ICM and FCM and CVs were the lowest. This optimal concentration was determined empirically for the cell concentrations used in this study (2.6 x 10^5 *K. veneficum* cells mL^{-1} and 1 x 10^5 calf thymocyte nuclei mL^{-1}).

Cell cycle deconvolution of DNA histograms

Cell cycle analysis of culture samples stained with 1 µg mL^{-1} DAPI were in agreement between the FCM and ICM data, and G1 peak CVs were comparable between the two methods (Fig. 6, Table 2). The ICM average *K. veneficum* G1 peak CV was 6.4 ± 1.1 %, while the FCM average *K. veneficum* G1 peak CV was 5.2 ± 0.4 %. These CVs were not significantly different (p-value = 0.16). Increasing the event total to 10,000 events for FCM analyses resulted in a reduction of *K. veneficum* G1 peak CV to 4.7 ± 0.1 % (data not shown). The average CVs for the calf thymocyte nuclei within the dinoflagellate sample analyzed by ICM were 12.8 ± 1.7 %, and the average FCM CVs were 3.3 ± 0.6 % which were significantly different (p-value < 0.01). Two-way ANOVA indicated no statistical difference in cell cycle phase distributions between

the two methods of analysis (p-value = 0.93). Additionally, the statistical test revealed that differences between cell cycle phases (i.e. G1 vs S vs G2 + M) were significant (p-value < 0.001) and there were no significant interactions between cytometry method and cell cycle phase (p-value = 0.07).

Comparative cell cycle analysis of the natural bloom sample by ICM versus FCM demonstrated some significant differences. Apparent precision in measuring G1-phase DNA content was significantly better for FCM analysis (G1 peak CV = 6.4 %) than ICM analysis (G1 peak CV = 10.3 %). However, deconvolution of cell cycle phases was successful for both methods (Fig. 7). Deconvolution of ICM data estimated 85.5 ± 1.1 % of the *K. veneficum* cells to be in G1-phase, 1.0 ± 0.3 % in S-phase, and 13.5 ± 1.0 % in G2 + M-phase. This contrasted with deconvolution of FCM data that estimated 73.9 ± 1.3 % of the *K. veneficum* cells to be in G1-phase, 5.2 ± 0.7 % to be in S-phase, and 20.9 ± 1.2 % to be in G2 + M-phase. Comparison of corresponding cell cycle phase frequencies revealed significant differences between ICM and FCM (Z-test, p-value < 0.001). Additionally, DNA indices (G2 mean: G1 mean) for the two data sets were not in agreement; with an ICM DNA index of 1.9 and an FCM DNA index of 1.6.

Discussion

ICM has been used in a very limited number of phytoplankton and fungal studies (Gisselson et al., 1999, Kullman & Teterin, 2006, Von Dassow et al., 2008), these have generally lacked detailed methods and give little information on quantitative precision. However, ICM has been extensively utilized and optimized for clinical research (Poulin et al., 1994a, Poulin et al.,

1994b, Wang et al., 1995, Maciorowski et al., 1997, Varga et al., 2004, Roukos et al., 2015). Such studies largely informed the methods developed here. Overall, ICM data obtained here for the dinoflagellate *K. veneficum*, were of equivalent or higher quality in terms of DNA peak CV's as those reported in clinical studies on human cells where CVs ranged from 3.5 % to 16.4 % (Lamas et al., 2003 and references above).

The CVs for *K. veneficum* 1C DNA peaks were comparable between both methods (ICM and FCM) and other ICM studies, which range from 3.4 % to 16.6 % (Poulin et al., 1994a, Poulin et al., 1994b, Wang et al., 1995, Maciorowski et al., 1997, Lamas et al., 2003). In Maciorowski et al. (1997), where fixation and slide mounting methods were compared; the best CV attained was 6.1 % which is only slightly better than CVs reported here (human peripheral blood lymphocytes, 1C DNA = 3.5 pg DNA, n = 200). Poulin et al. (1994b) achieved CVs as low as 3.4 % in ethanol fixed propidium iodide stained human adenocarcinoma cells (n = 1000). In comparison to previous phytoplankton studies, the CVs reported here using ICM are comparable to other studies using microfluorometry (3.6 % - 9.1 %) (Chang & Carpenter, 1988, Cetta & Anderson, 1990, Yamaguchi, 1992) and FCM (7.3 % -12.1 %) (Parrow & Burkholder, 2003a, Parrow & Burkholder, 2003b, Figueroa et al., 2010). *Karlodinium veneficum* genome size estimations determined by ICM in this study (13.8 ± 2.3 pg DNA $cell^{-1}$ to 14.6 ± 1.5 pg DNA $cell^{-1}$) are also comparable to those reported for other North American strains, which ranged from 11.2 ± 0.6 pg DNA $cell^{-1}$ to 16.9 pg DNA $cell^{-1}$ (LaJeunesse et al., 2005, Adolf et al., 2020). Interestingly, DAPI titrations revealed fluorescence intensity ratios between *K. veneficum* nuclei and calf thymocyte nuclei were less perturbed by increasing dye concentrations when analyzed by ICM as opposed to FCM. The effect of DAPI concentration on mean fluorescence intensity and CVs have previously been reported (Yamaguchi, 1992, Wen et al., 2001). Wen et

al. (2001), using FCM, observed increases in both CVs and mean fluorescence intensity of trout red blood cell standards and mouse cell lines with increased DAPI concentrations. This was attributed to oversaturation of DAPI and was reversible by dilution of cell suspensions in DAPI free buffer. Additionally, they observed an effect of staining buffer pH on CVs for mouse cell lines, concluding pH = 6 to be optimal for DAPI staining. Yamaguchi (1992), using microfluorometry to study the cell cycle of *Gymnodinium nagasakiense* (= *Karenia mikimotoi*), also observed effects of DAPI concentration on both CVs and mean fluorescence intensity. The differences observed in this current study between ICM and FCM in terms of stain type and concentration are likely due to the unavoidable differences between ICM and FCM sample preparation. Samples prepared for ICM were fully dried onto coverslips. This may lead to altered hydration states of DNA and DAPI or SYBR Green I molecules, possibly leading to conformational changes that alter dye binding chemistry and/or fluorescence yield.

The determined CVs of the calf thymocyte nuclei standards in ICM were higher than FCM, which may be explained by the different morphological dimensions of *K. veneficum* cells (8 – 12 μm, Place et al., 2012) versus calf thymocyte nuclei (~ 5 μm, Hess & Lagg, 1958), when stained and analyzed together as internal standards in ICM images. This was supported by the observation that when calf thymocyte nuclei were analyzed alone by ICM, CVs were as low as 6.2 % (data not shown). As previously reported in Lockett et al. (1992) and Varga et al. (2004) the z-axis distance from the optimal focal plane of fluorescent objects has a significant impact on the precision of fluorescence measurement in ICM. This effect is largely influenced by the focal depth of the objective used, which is inversely proportional to the square of the numerical aperture (Waters, 2009). In the case of the objective used here (20x, NA = 0.8) the theoretical focal depth is approximately 1.6 μm which is less than the difference in diameters of the *K.*

veneficum cells and calf thymocyte nuclei. Therefore, collecting images in the optimal focal plane for *K. veneficum* cells inevitably resulted in suboptimal focus for the calf thymocyte nuclei, which increased their CV's as compared to FCM. Likewise, use of high ionic strength buffer in slide preparation was found to exacerbate focal plane differences, as salt precipitation during sample drying resulted in specimens being distributed amongst multiple focal planes, which increased CV's in ICM. The method described here minimizes the effects of multiple focal planes by using poly-D-lysine coated coverslips and a low ionic strength resuspension/slide preparation solution (i.e. Milli-Q H_2O), thereby reducing the number of out of focus specimens. Lastly, increasing objective magnification and NA was observed to contribute to increases in fluorescent measurement error in ICM, due to decreasing focal depth for reasons given above. Therefore a compromise must be made in selecting the appropriate magnification that facilitates user discrimination of non-target taxa while also attaining the highest practical level of precision in DNA fluorescence measurement. In this study, the 20x objective was found to be a good compromise that allowed easy discrimination of *K. veneficum* cells from other similarly sized taxa, which would prove more difficult with a lower powered (e.g. 10x) objective.

At this time, we know of no epifluorescence light source and/or optics system that can deliver a completely flat, uniform field of epi-illumination across a microscope field of view, at all magnifications. Therefore, flatfield correction was found to be necessary for precision in ICM using widefield fluorescence microscopy (Lockett et al., 1992, Model & Burkhardt, 2001). Following flatfield correction, precision of fluorescence intensity measurements via ICM for both microsphere and nuclear DNA standards improved significantly and became comparable to that of FCM analysis. Coefficients of variation obtained herein on fluorosphere standards were 2.1%, consistent with previous ICM studies where such CVs ranged from 2 % to 3.9 % (Lockett

et al., 1992, Poulin et al., 1994a, Poulin et al., 1994b, Varga et al., 2004). All of these studies used a flatfield correction method similar to that used here, although Poulin et al. (1994a), additionally improved CV's of fluorosphere standards from 2.7% to 2% by setting the field aperture of the epi-source to half stop, thereby reducing the effects of glare, but reducing the useable frame of the CCD camera to one quarter of its original size. This would have had the disadvantage of significantly impacting the speed of data acquisition.

Using methods optimized here, ICM was shown to be equivalent to FCM for determining DNA content and cell cycle phase distribution in cultured *K. veneficum*, with no significant differences found between identical samples analyzed using the two different platforms. This clearly demonstrates the comparability of ICM to FCM for cell cycle analysis, in agreement with clinical studies comparing ICM to FCM for cell cycle/ploidy analysis of human lymphocyte cells, as well as tumors from lung and breast cancer patients (Montironi et al., 1993, Yamamoto et al., 1994, Chan et al., 2011). Unlike culture samples, *K. veneficum* cell cycle phase distributions in the field bloom sample were less close in agreement between ICM and FCM estimates. This was likely a result of variation introduced during sample preparation that caused increased cell clumping during slide preparation (Fig. 8) as compared to the culture samples. Unlike culture samples, the field sample had been in storage for a long period of time (years) before analysis. This may have caused the observed increased cell clumping, which had the effect in ICM of distributing many/most cells through slightly different focal planes, which increased error in DNA fluorescence measurements for reasons given above. This problem should be correctable in the future through timelier sample analysis and/or increased physical disaggregation steps. Clumped cells were automatically excluded from analysis in FCM via gated size exclusion, and the method allowed a much larger volume of sample to be analyzed to

gradually collect data from (relatively rare) non-clumped cells. The exclusion gates in ICM could have also been adjusted for a higher degree of exclusion, but changing such parameters mid-experiment was against the goals of this study. Overall, ICM appeared to slightly overestimate the percentage of G1-phase cells in bloom samples, and thus underestimated S and G2 + M phase cells as compared to FCM. This was likely caused by the higher G1 CV in the ICM DNA histogram, which the cell cycle model accommodated with a wider Gaussian fit, thereby overlapping a portion of the S-phase population. While the ICM G1 peak CV (10.3 %) was higher than the FCM CV (6.4 %) for the field samples, it nevertheless fell within an acceptable range (< 15 %) (Boucher et al., 1991, Veldhuis et al., 1997, Ormerod et al., 1998, Parrow & Burkholder, 2003a). Furthermore, CVs are typically not reported for field data on bloom cell cycle phase distribution (Vaulot & Partensky, 1992, Garcés et al., 1998, Garcés et al., 1999, Garcés & Masó, 2001). Even if the case, overestimation of the percentage of G1-phase cells when determining in situ growth rates would only result in a lower (i.e. more conservative) estimate of specific growth rates (μ).

This study demonstrates that ICM can be an effective technique for performing nuclear genome size estimations and cell cycle analysis of microalgal taxa in culture and natural bloom populations including phagotrophic species and complex field assemblages which present particular problems for FCM. As with other quantitative fluorescence microscopy methods, several important factors need to be considered for acquiring precise measurements in ICM (Waters, 2009): 1) uniformity of illumination or image correction, 2) careful selection of a fluorochrome with regards to binding specificity, quantum yield, and Stoke's shift, 3) saturation of fluorochrome binding, 4) fluorescence fading, 5) characteristics of the microscope objective such as magnification and numerical aperture, and 6) signal to noise ratio and linearity of the

camera used to capture images. These factors were critical to the development of the methods optimized here for *K. veneficum*, and future studies should carefully consider other factors such as cell concentration and stain incubation time when determining optimal dye concentrations (Kremp & Parrow, 2006, Darzynkiewicz, 2011).

Theoretical advantages of ICM over classical microfluorometry include much more rapid data acquisition and data archiving as images. Potential advantages over flow cytometry include reduced instrumentation costs and maintenance, ability to visually select cells of interest by morphology, and ability to measure nuclear DNA while ignoring cytoplasmic DNA (or vice versa). Data collection and processing in ICM can proceed rapidly, with the data from the bloom sample in this study collected as only 15 images with an average of 77.1 cells analyzed per image. Data on cultured samples was collected as ~ 11 images per replicate, with an average of~ 235 cells per image using the 20x objective. Analysis of the images was rapid and automatically performed by the trained image analysis software. The rate of processing was primarily slowed by user curation to manually remove non-target nuclei (e.g. other phytoplankton with similar genome sizes, intracellular food vacuoles containing ingested nuclei) from the analyses. Application in field samples was aided by the ability to use morphological identification in brightfield images that were cross-referenced to their respective fluorescent images being analyzed (Fig. 8).

Although this study made use of a commercially available image analysis software package (Zen 2.6), other image analysis tools are available that could be also be utilized in ICM. Wiesmann et al. (2015) reviewed 15 free image analysis software tools, and ranked them based on usability and functionality. Of these, CellProfiler was specifically designed for high-throughput image analysis (Kamentsky et al., 2011). This software allows user designed analysis

pipelines that can be utilized to analyze hundreds of images automatically. This could significantly improve data collection speeds as compared to Zen 2.6, which required analysis of a single image at a time.

With the methods and tools described by this study and references within, ICM can be adopted from clinical research into ecological field studies to measure cell cycle progression and in situ growth rates of natural bloom populations of complex assemblages and/or phagotrophic/mixotrophic microalgae. Furthermore, multiparameter fluorescence studies are possible with ICM (Galbraith et al., 1991). The application of multiparameter fluorescence would be useful for investigating the cell cycle progression in relation to other labelled biomarkers, including those labelled using immunofluorescence and fluorescence in situ hybridization. This could be useful for studies of other biotic factors influencing bloom formation, maintenance, and decline such as co-occurrence of intracellular parasites like *Amoebophrya* that have been implicated in the demise of *K. veneficum* blooms (Place et al., 2012). One such a study was previously performed during an *Alexandrium fundyense* bloom using an Imaging FlowCytobot modified specifically for measuring cellular DNA content (Brosnahan et al., 2014). This type of study was complicated by instrumentation expense, necessary expertise, and the inability to ignore cytoplasmic/vacuolar DNA. Image cytometry offers a cost effective, accessible, alternative platform for cell cycle and other quantitative fluorescence-based studies of both cultured mixotrophic/phagotrophic microalgae and complex natural field populations.

Acknowledgments

This research was supported by the National Oceanic and Atmospheric Administration, National Centers for Coastal Ocean Science ECOHAB Program, grant number NA15NOS4780180. The authors acknowledge the assistance of Dr. Saddef Haq in obtaining the Baltimore Harbor bloom sample. The authors would like to extend appreciation to Richard Riese of Biosure® Inc. for assistance with cytometry DNA standards. This paper is ECOHAB contribution No. 969, No. 5887 from the University of Maryland Center for Environmental Science, and No. 20-013 from the Institute of Marine and Environmental Technology.

REFERENCES CITED

Adolf, J. E., Bachvaroff, T. R. & Place, A. R. 2009. Environmental modulation of karlotoxin levels in strains of the cosmopolitan dinoflagellate, *Karlodinium veneficum* (Dinophyceae). *J. Phycol.* **45**:176-92.

Adolf, J. E., Parrow, M. W. & Place, A. R. 2020. *Karlodinium veneficum*: Still blooming and toxic sixty-two years later. *In*: Subba Rao, V. D. [Ed.] *Dinoflagellates.* Nova Science Publishers, Inc., pp. 355 - 402.

Bachvaroff, T. R., Adolf, J. E., Squier, A. H., Harvey, H. R. & Place, A. R. 2008. Characterization and quantification of karlotoxins by liquid chromatography-mass spectrometry. *Harmful Algae* **7**:473-84.

Berges, J. A., Franklin, D. J. & Harrison, P. J. 2001. Evolution of an artificial seawater medium: Improvements in enriched seawater, artificial water over the last two decades. *J. Phycol.* **37**:1138-45.

Bhaud, Y., Salmon, J.-M. & Soyer-Gobillard, M.-O. 1991. The complex cell cycle of the dinoflagellate protoctist *Crypthecodinium cohnii* as studied *in vivo* and by cytofluorimetry. *J. Cell Sci.* **100**:675-82.

Bocsi, J., Varga, V. S., Molnár, B., Sipos, F., Tulassay, Z. & Tárnok, A. 2004. Scanning fluorescent microscopy analysis is applicable for absolute and relative cell frequency determinations. *Cytometry Part A* **61A**:1-8.

Boucher, N., Vaulot, D. & Partensky, F. 1991. Flow cytometric determination of phytoplankton DNA in cultures and oceanic populations. *Mar. Ecol. Prog. Ser.* **71**:75-84.

Brosnahan, M. L., Farzan, S., Keafer, B. A., Sosik, H. M., Olson, R. J. & Anderson, D. M. 2014. Complexities of bloom dynamics in the toxic dinoflagellate *Alexandrium fundyense* revealed through DNA measurements by imaging flow cytometry coupled with species-specific rRNA probes. *Deep Sea Res. Part II Top. Stud. Oceanogr.* **103**:185-98.

Carpenter, E. J. & Chang, J. 1988. Species-specific phytoplankton growth rates via diel DNA synthesis cycles. I. Concept of the method. *Mar. Ecol. Prog. Ser.* **43**:105-11.

Cetta, C. M. & Anderson, D. M. 1990. Cell cycle studies of the dinoflagellates *Gonyaulax polyedra* Stein and *Gyrodinium uncatenum* Hulburt during asexual and sexual reproduction. *J. Exp. Mar. Biol. Ecol.* **135**:69-83.

Chan, L. L., Zhong, X., Qiu, J., Li, P. Y. & Lin, B. 2011. Cellometer Vision as an alternative to flow cytometry for cell cycle analysis, mitochondrial potential, and immunophenotyping. *Cytometry Part A* **79A**:507-17.

Chang, J. & Carpenter, E. J. 1988. Species-specific phytoplankton growth rates via diel DNA synthesis cycles. II. DNA quantification and model verification in the dinoflagellate *Heterocapsa triquetra*. *Mar. Ecol. Prog. Ser.* **44**:287-96.

Chang, J. & Dam, H. G. 1993. The influence of grazing on the estimation of phytoplankton growth rate via cell cycle analysis: experimental and modeling evidence. *Limnol. Oceanogr.* **34**:202-12.

Darzynkiewicz, Z. 2011. Critical aspects in analysis of cellular DNA content. *Curr. Protoc. Cytom.* **56**:7.2.1-7.2.8.

Deeds, J. R., Kibler, S. R., Tester, P. A. & Place, A. R. 2004. Geographic strain variation in toxin production in *Karlodinium micrum* (Dinophyceae) from Southeastern United States. *In*:

Steidinger, K. A., Landsberg, J. H., Tomas, C. R. & Vargo, G. A. [Eds.] *Harmful Algae 2002.* IOC-UNESCO, Florida, pp. 145-47.

Deeds, J. R. & Place, A. R. 2006. Sterol-specific membrane interactions with the toxins from *Karlodinium micrum* (Dinophyceae) — a strategy for self-protection? *Afr. J. Mar. Sci.* **28**:421-25.

Deeds, J. R., Terlizzi, D. E., Adolf, J. E., Stoecker, D. K. & Place, A. R. 2002. Toxic activity from cultures of *Karlodinium micrum* (=*Gyrodinium galatheanum*) (Dinophyceae)—a dinoflagellate associated with fish mortalities in an estuarine aquaculture facility. *Harmful Algae* **1**:169-89.

Figueroa, R. I., Garcés, E. & Bravo, I. 2010. The use of flow cytometry for species identification and life-cycle studies in dinoflagellates. *Deep Sea Res. Part II Top. Stud. Oceanogr.* **57**:301-07.

Galbraith, W., Wagner, M. C. E., Chao, J., Abaza, M., Ernst, L. A., Nederlof, M. A., Hartsock, R. J., Taylor, D. L. & Waggoner, A. S. 1991. Imaging cytometry by multiparameter fluorescence. *Cytometry* **12**:579-96.

Garcés, E., Delgado, M., Masó, M. & Camp, J. 1998. Life history and in situ growth rates of *Alexandrium taylori* (Dinophyceae, Pyrrophyta). *J. Phycol.* **34**:880-87.

Garcés, E., Delgado, M., Masó, M. & Camp, J. 1999. In situ growth rate and distribution of the ichthyotoxic dinoflagellate *Gyrodinium corsicum* Paulmier in an estuarine embayment (Alfacs Bay, NW Mediterranean Sea). *J. Plankton Res.* **21**:1977-91.

Garcés, E. & Masó, M. 2001. Phytoplankton potential growth rate versus increase in cell numbers estimation of cell lysis. *Mar. Ecol. Prog. Ser.* **212**:297-300.

Gisselson, L.-Å., Granéli, E. & Carlsson, P. 1999. Using cell cycle analysis to estimate in situ growth rate of the dinoflagellate *Dinophysis acuminata*: drawbacks of the DNA quantification method. *Mar. Ecol. Prog. Ser.* **184**:55-62.

Hess, E. L. & Lagg, S. E. 1958. Calf thymus composition: a comparison of differential centrifugation and chemical fractionation procedures. *J. Biophys. Biochem. Cytol.* **4**:717-25.

Kamentsky, L., Jones, T. R., Fraser, A., Bray, M.-A., Logan, D. J., Madden, K. L., Ljosa, V., Rueden, C., Eliceiri, K. W. & Carpenter, A. E. 2011. Improved structure, function and compatibility for CellProfiler: modular high-throughput image analysis software. *Bioinformatics* **27**:1179-80.

Kapraun, D. F. & Freshwater, D. W. 2012. Estimates of nuclear DNA content in red algal lineages. *AoB Plants* **2012**:pls005-pls05.

Kempton, J. W., Lewitus, A. J., Deeds, J. R., Law, J. M. & Place, A. R. 2002. Toxicity of *Karlodinium micrum* (Dinophyceae) associated with a fish kill in a South Carolina brackish retention pond. *Harmful Algae* **1**:233-41.

Kremp, A. & Parrow, M. W. 2006. Evidence for asexual resting cysts in the life cycle of the marine peridinoid dinoflagellate, *Scrippsiella hangoei*. *J. Phycol.* **42**:400-09.

Kullman, B. & Teterin, W. 2006. Estimation of fungal genome size: comparison of image cytometry and photometric cytometry. *Folia Cryptogam. Est.* **42**:43-56.

LaJeunesse, T. C., Lambert, G., Andersen, R. A., Coffroth, M. A. & Galbraith, D. W. 2005. *Symbiodinium* (Pyrrhophyta) genome sizes (DNA content) are smallest among dinoflagellates. *J. Phycol.* **41**:880-86.

Lamas, E., Chassoux, D., Decaux, J.-F. o., Brechot, C. & Debey, P. 2003. Quantitative fluorescence imaging approach for the study of polyploidization in hepatocytes. *J. Histochem. Cytochem.* **51**:319-30.

Lim, H. C., Leaw, C. P., Tan, T. H., Kon, N. F., Yek, L. H., Hii, K. S., Teng, S. T., Razali, R. M., Usup, G., Iwataki, M. & Lim, P. T. 2014. A bloom of *Karlodinium australe* (Gymnodiniales, Dinophyceae) associated with mass mortality of cage-cultured fishes in West Johor Strait, Malaysia. *Harmful Algae* **40**:51-62.

Litaker, R. W., Warner, V. E., Rhyne, C., Duke, C. S., Kenney, B. E., Ramus, J., Tester, P. A. 2002. Effect of diel and interday variations in light on the cell division pattern and in situ growth rates of the bloom-forming dinoflagellate *Heterocapsa triquetra*. *Mar. Ecol. Prog. Ser.* **232:**63-74.

Liu, H., Campbell, L., Landry, M. R., Nolla, H. A., Brown, S. L. & Constantinou, J. 1998. *Prochlorococcus* and *Synechococcus* growth rates and contributions to production in the Arabian Sea during the 1995 Southwest and Northeast Monsoons. *Deep Sea Res. Part II Top. Stud. Oceanogr*. **45**:2327-52.

Liu, H., Nolla, H. A. & Campbell, L. 1997. *Prochlorococcus* growth rate and contribution to primary production in the equatorial and subtropical North Pacific Ocean. *Aquat. Microb. Ecol.* **12**:39-47.

Lockett, S. J., Jacobson, K. & Herman, B. 1992. Quantitative precision of an automated, fluorescence-based image cytometer. *Anal. Quant. Cytol. Histol.* **14**:187-202.

Maciorowski, Z., Veilleux, C., Gibaud, A., Bourgeois, C. A., Klijanienko, J., Boenders, J. & Vielh, P. 1997. Comparison of fixation procedures for fluorescent quantitation of DNA content using image cytometry. *Cytometry* **28**:123-29.

Malpica, N., de Solórzano, C. O., Vaquero, J. J., Santos, A., Vallcorba, I., García-Sagredo, J. M. & del Pozo, F. 1997. Applying watershed algorithms to the segmentation of clustered nuclei. *Cytometry* **28**:289-97.

McDuff, R. E. & Chisholm, S. W. 1982. The calculation of in situ growth rates of phytoplankton populations from fractions of cells undergoing mitosis: A clarification. *Limnol. Oceanogr.* **27**:783-88.

Model, M. A. & Burkhardt, J. K. 2001. A standard for calibration and shading correction of a fluorescence microscope. *Cytometry* **44**:309-16.

Montironi, R., Diamanti, L., Santinelli, A., Magi Galluzzi, C., Scarpelli, M., Giannulis, I. & Mangili, F. 1993. Computed cell cycle and DNA histogram analyses in image cytometry in breast cancer. *J. Clin. Pathol.* **46**:795-800.

Ormerod, M. G., Tribukait, B. & Giaretti, W. 1998. Consensus report of the task force on standardisation of DNA flow cytometry in clinical pathology. DNA Flow Cytometry Task Force of the European Society for Analytical Cellular Pathology. *Anal. Cell. Pathol.* **17**:103-10.

Otsu, N. 1979. A threshold selection method from gray-level histograms. *IEEE Trans. Syst. Man Cybern.* **9**:62-66.

Parrow, M. W. & Burkholder, J. M. 2003a. Estuarine heterotrophic cryptoperidiniopsoids (Dinophyceae): Life cycle and culture studies. *J. Phycol.* **39**:678-96.

Parrow, M. W. & Burkholder, J. M. 2003b. Reproduction and sexuality in *Pfiesteria shumwayae* (Dinophyceae). *J. Phycol.* **39**:697-711.

Place, A. R., Bowers, H. A., Bachvaroff, T. R., Adolf, J. E., Deeds, J. R. & Sheng, J. 2012. *Karlodinium veneficum*—The little dinoflagellate with a big bite. *Harmful Algae* **14**:179-95.

Poulin, N., Harrison, A. & Palcic, B. 1994a. Quantitative precision of an automated image cytometric system for the measurement of DNA content and distribution in cells labeled with fluorescent nucleic acid stains. *Cytometry* **16**:227-35.

Poulin, N. M., Matthews, J. B., Skov, K. A. & Palcic, B. 1994b. Effects of fixation method on image cytometric measurement of DNA content and distribution in cells stained for fluorescence with propidium iodide. *J. Histochem. Cytochem.* **42**:1149-56.

Roukos, V., Pegoraro, G., Voss, T. C. & Misteli, T. 2015. Cell cycle staging of individual cells by fluorescence microscopy. *Nat. Protoc.* **10**:334.

Salvador Soler, N., Gómez Garreta, A., Ribera Siguan, M. A. & Kapraun, D. F. 2014. Nuclear DNA content variation in life history phases of the Bonnemasoniaceae (Rhodophyta). *PLOS ONE* **9**:e86006.

Van Dolah, F. M. & Leighfield, T. A. 1999. Diel phasing of the cell-cycle in the Florida red tide dinoflagellate, *Gymnodinium breve*. *J. Phycol.* **35**:1404-11.

Van Dolah, F. M., Leighfield, T. A., Kamykowski, D., Kirkpatrick, G. J. 2008. Cell cycle behavior of laboratory and field populations of the Florida red tide dinoflagellate, *Karenia brevis*. *Cont. Shelf Res.* **28**:11-23.

Van Wagoner, R. M., Deeds, J. R., Satake, M., Ribeiro, A. A., Place, A. R. & Wright, J. L. C. 2008. Isolation and characterization of karlotoxin 1, a new amphipathic toxin from *Karlodinium veneficum*. *Tetrahedron Lett.* **49**:6457-61.

Varga, V. S., Bocsi, J., Sipos, F., Csendes, G., Tulassay, Z. & Molnár, B. 2004. Scanning fluorescent microscopy is an alternative for quantitative fluorescent cell analysis. *Cytometry Part A* **60A**:53-62.

Vaulot, D. 1992. Estimate of phytoplankton division rates by the mitotic index method: The fmax approach revisited. *Limnol. Oceanogr.* **37**:644-49.

Vaulot, D. & Partensky, F. 1992. Cell cycle distributions of prochlorophytes in the north western Mediterranean Sea. *Deep Sea Res. A* **39**:727-42.

Veldhuis, M. J. W., Cucci, T. L. & Sieracki, M. E. 1997. Cellular DNA content of marine phytoplankton using two new fluorochromes: Taxonomic and ecological implications. *J. Phycol.* **33**:527-41.

Vinogradov, A. E. 1998. Genome size and GC-percent in vertebrates as determined by flow cytometry: The triangular relationship. *Cytometry* **31**:100-09.

Von Dassow, P., Petersen, T. W., Chepurnov, V. A. & Armbrust, E. V. 2008. Inter- and intraspecific relationships between nuclear DNA content and cell size in selected members of the centric diatom genus *Thalassiosira* (Bacillariophyceae). *J. Phycol.* **44**:335-49.

Wang, N., Pan, Y., Heiden, T. & Tribukait, B. 1995. Fluorescence image cytometry for measurement of nuclear DNA content in surgical pathology. *Cytometry* **22**:323-29.

Waters, J. C. 2009. Accuracy and precision in quantitative fluorescence microscopy. *J. Cell Biol.* **185**:1135-48.

Watson, J. V., Chambers, S. H. & Smith, P. J. 1987. A pragmatic approach to the analysis of DNA histograms with a definable G1 peak. *Cytometry* **8**:1-8.

Wen, J., Krishan, A. & Thomas, R. A. 2001. NASA/American Cancer Society high-resolution flow cytometry project – II. Effect of pH and DAPI concentration on dual parametric analysis of DNA/DAPI fluorescence and electronic nuclear volume. *Cytometry* **43**:12-15.

Wiesmann, V., Franz, D., Held, C., Münzenmayer, C., Palmisano, R. & Wittenberg, T. 2015. Review of free software tools for image analysis of fluorescence cell micrographs. *J. Microsc.* **257**:39-53.

Yamaguchi, M. 1992. DNA synthesis and the cell cycle in the noxious red-tide dinoflagellate *Gymnodinium nagasakiense*. *Mar. Biol.* **112**:191-98.

Yamamoto, T., Horiguchi, H., Kamma, H., Noro, M., Ogata, T., Inage, Y., Akaogi, E., Mitsui, K., Hori, M. & Isobe, M. 1994. Comparative DNA analysis by image cytometry and flow cytometry in non-small cell lung cancer. *Jap. J. Cancer Res.* **85**:1171-77.

FIGURE LEGENDS

Figure 1. Field of view captured from an epifluorescence illuminated film of fluorescein. Fluorescence patterns before (A) and after (B) flatfield correction, with respective 2.5 dimensional representations (C and D). Z-axis in 2.5 dimensional representations indicate pixel gray level. X and Y axes indicate X/Y position within field of view.

Figure 2. Fluorescence histograms of Flow-Check™ fluorospheres (n = 1373 events), analyzed by image cytometry prior to flatfield correction (A), after flatfield correction (B), and by flow cytometry (C).

Figure 3. Comparison of FCM (A-C) and ICM (D-F) DNA histograms stained with 5x SYBR® Green I (A and D), 20x SYBR® Green I (B and E), and 1 μg mL^{-1} DAPI (C and F). Calf thymocyte nuclei (CTNs; diagonal stripe fill) used as genome size standards for estimating *K. veneficum* (solid gray fill) 1C DNA content (n = 2500 events). Higher magnitude values on the X-axis scale of ICM histograms are due to greater dynamic range for the CCD camera as compared to the FCM photomultiplier tubes.

Figure 4. Crosswise comparison of the effects of objective magnification (10x, 20x, 40x) and cell resuspension/slide preparation solution (Milli-Q H_2O versus TE) on 1C DNA peak CV's measured by ICM. Scales of X-axes vary due to differences in number of pixels per nucleus as a factor of magnification.

Figure 5. The effect of DAPI concentration on genome size estimation for *K. veneficum*, as measured by FCM (light gray) versus ICM (dark gray). Error bars represent ± 1 SD, which were propagated from % CVs of calf thymocyte nuclei and *K. veneficum* 1C DNA peaks (n = 2500 events).

Figure 6. Representative DNA histograms from ICM (A) and FCM (B) analysis of the same culture replicate fitted to Watson-Pragmatic cell cycle model. Overlay of Watson Pragmatic cell cycle model is shown, where the proportion of G1-phase is represented with dark gray shading, S-phase is represented with black shading, and G2-phase is represented by light gray shading (n = 2500 events). Deconvolved percentages do not account for population overlaps between G1 and S phases or S and G2 + M phases. X-axis scale differences due to the dynamic range of the CCD camera (ICM) versus photomultiplier tube (FCM).

Figure 7. Representative DNA histograms from a natural bloom sample; Watson-Pragmatic deconvolution of ICM (A) and FCM (B) collected data (n = 1157 events). Deconvolved percentages do not account for population overlaps between G1 and S phases or S and G2 + M phases. X-axis scale differences due to the dynamic range of the CCD camera (ICM) versus photomultiplier tube (FCM).

Figure 8. Matching epifluorescence (A and B) and brightfield (C and D) images from a *K. veneficum* bloom sample (A and C) and culture (B and D) used for ICM analysis. Calf thymocyte nuclei (red arrowheads) included in *K. veneficum* culture sample as internal DNA standard. In

focus *K. veneficum* cells (white arrowheads) and non-target taxa (arrows) are identified using the brightfield image and included/excluded from analysis of the epifluorescence image. Cell clumping (white circles) and out of focus *K. veneficum* cells (notched arrowheads) contributed to the variability of ICM measurements. All images captured at 20x objective magnification. Scale bar = 50 μm.

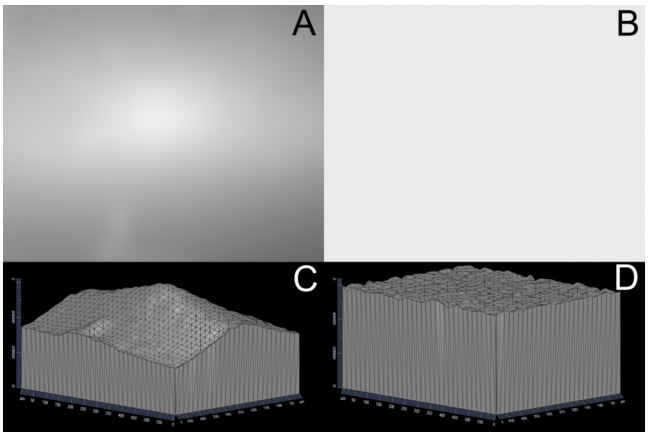

LOM3_10420_Figure_1.tif

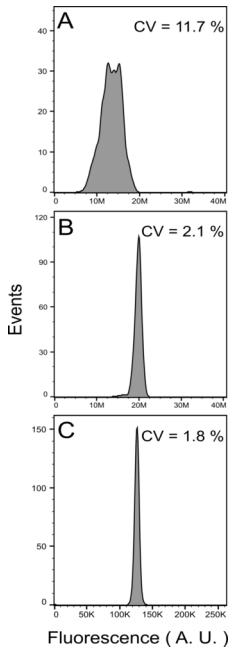

LOM3_10420_Figure_2.tif

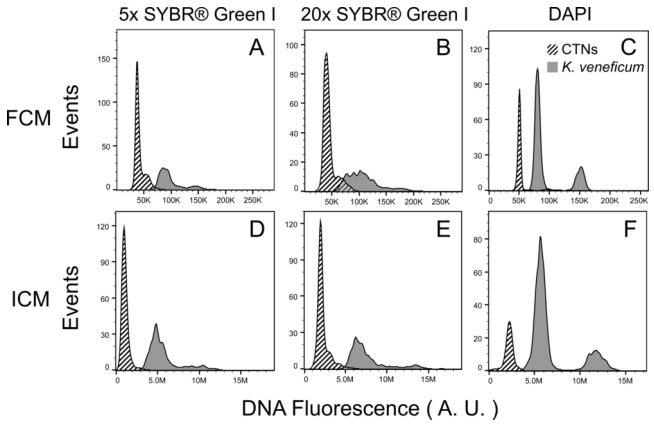

LOM3_10420_Figure_3.tif

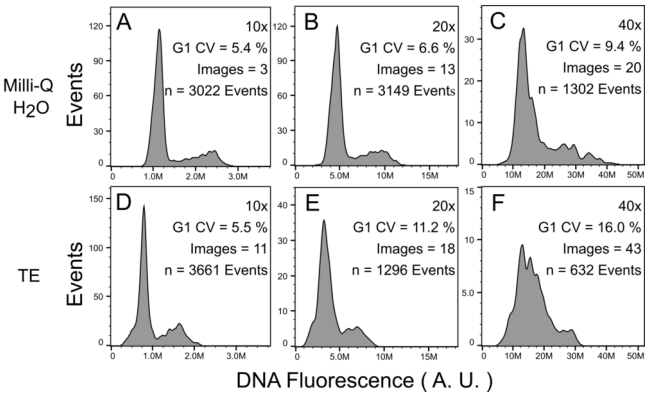

LOM3_10420_Figure_4.tif

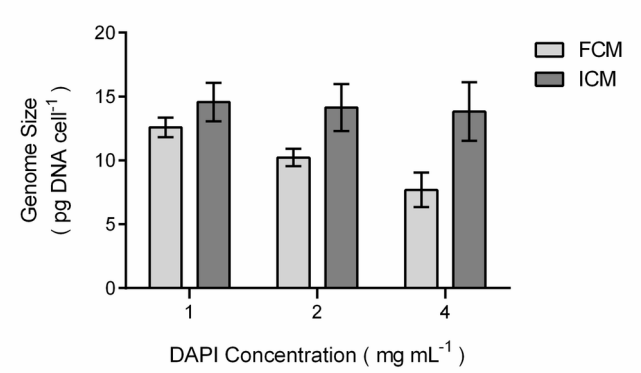

LOM3_10420_Figure_5.tif

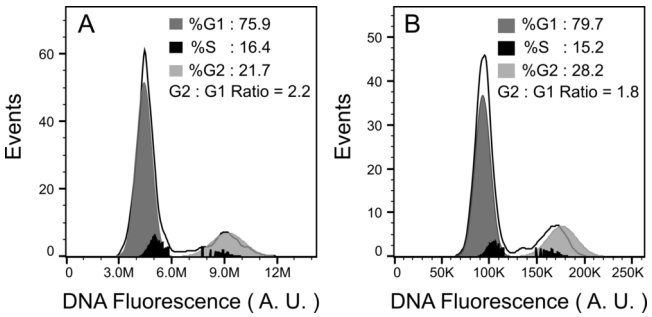

LOM3_10420_Figure_6.tif

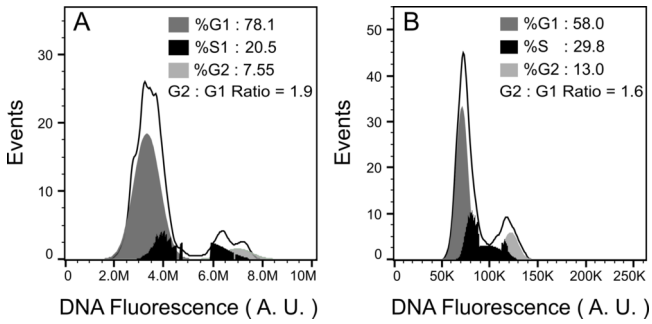

LOM3_10420_Figure_7.tif

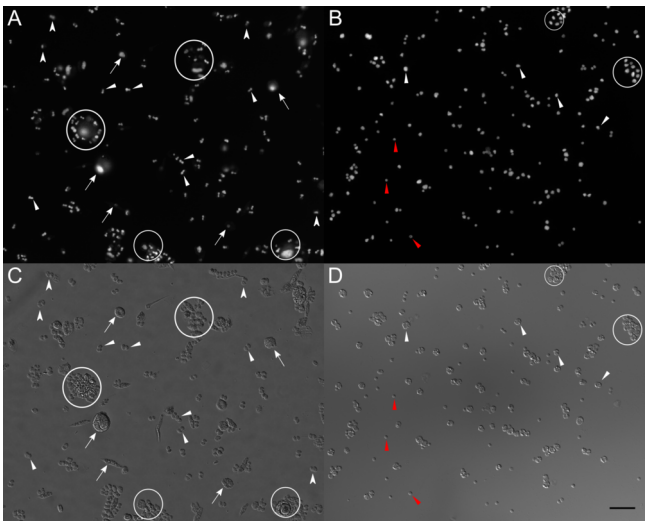

LOM3_10420_Figure_8.tif

Table 1: Comparison of precision and genome size estimation by ICM and FCM using SYBR® Green I (5x and 20x concentrations) and DAPI (1 μg mL^{-1}) nucleic acid dyes. Genome size standard deviations propagated from % CVs of calf thymocyte nuclei (CTN) and *K. veneficum* 1C DNA peaks (n = 2500 events). Highlighted genome estimations were in agreement with reports from other North American strains (LaJeunesse et al., 2005, Adolf et al., 2020).

Dye (Concentration)	Analysis Method	CTN (% CV)	*K. v.* G1 (% CV)	*K. v.* 1C/ CTN	*K. v.* Genome Size Estimation (pg DNA $cell^{-1}$ ± SD)
SYBR® Green (5x)	FCM	5.0	7.3	2.3	17.0 ± 1.5
	ICM	16.3	9.4	4.8	35.5 ± 3.9
SYBR® Green (20x)	FCM	8.7	16.6	2.4	17.8 ± 1.6
	ICM	8.1	7.9	3.2	23.7 ± 2.6
DAPI (1 μg mL^{-1})	FCM	2.5	3.3	1.6	11.8 ± 0.5
	ICM	9.4	5.8	2.5	18.5 ± 2.0

Table 2: Cell cycle statistics. Mean percentage of cell cycle phases G1, S, and G2 with mean % CVs of *K. veneficum* G1 phase and the calf thymocyte nuclei (CTN) internal DNA standard from triplicate samples analyzed by ICM and FCM. Errors are SD.

	% G1	% S	% G2	*K.v*. G1 % CV	CTN % CV
ICM	80.0 ± 1.2	9.7 ± 2.6	10.2 ± 1.5	6.4 ± 1.1	12.8 ± 1.7
FCM	77.3 ± 0.6	7.9 ± 3.5	14.4 ± 4.1	5.2 ± 0.4	3.3 ± 0.6